



**HAL**  
open science

## Holocene glacial oscillations in the Tyroler Valley ( NE Greenland)

Julia Garcia-Oteyza Ciria, Marc Oliva, David Palacios, José M. Fernández-Fernández, Irene Schimmelpfennig, Alicia Medialdea, Marcelo Fernandes, Santiago Giralt, Vincent Jomelli, Dermot Antoniades

► **To cite this version:**

Julia Garcia-Oteyza Ciria, Marc Oliva, David Palacios, José M. Fernández-Fernández, Irene Schimmelpfennig, et al.. Holocene glacial oscillations in the Tyroler Valley ( NE Greenland). Land Degradation and Development, 2023, 34 (9), pp.2589-2606. 10.1002/ldr.4633 . hal-04807913

**HAL Id: hal-04807913**

**<https://hal.science/hal-04807913v1>**

Submitted on 28 Nov 2024

**HAL** is a multi-disciplinary open access archive for the deposit and dissemination of scientific research documents, whether they are published or not. The documents may come from teaching and research institutions in France or abroad, or from public or private research centers.

L'archive ouverte pluridisciplinaire **HAL**, est destinée au dépôt et à la diffusion de documents scientifiques de niveau recherche, publiés ou non, émanant des établissements d'enseignement et de recherche français ou étrangers, des laboratoires publics ou privés.






Distributed under a Creative Commons Attribution - NonCommercial - NoDerivatives 4.0 International License

## RESEARCH ARTICLE

WILEY

# Holocene glacial oscillations in the Tyroler Valley (NE Greenland)

Julia Garcia-Oteyza Ciria<sup>1</sup>  | Marc Oliva<sup>1</sup>  | David Palacios<sup>2</sup>  |  
 José M. Fernández-Fernández<sup>2</sup> | Irene Schimmelpfennig<sup>3</sup> | Alicia Medialdea<sup>4</sup> |  
 Marcelo Fernandes<sup>5</sup> | Santiago Giralt<sup>6</sup> | Vincent Jomelli<sup>3</sup> | Dermot Antoniades<sup>7</sup> |  
 ASTER TEAM<sup>3,8</sup>

<sup>1</sup>Department of Geography, Universitat de Barcelona, Barcelona, Spain

<sup>2</sup>Department of Geography, Universidad Complutense de Madrid, Madrid, Spain

<sup>3</sup>Aix-Marseille Université, CNRS, IRD, INRAE, Coll. France, UM 34 CEREGE, Aix-en-Provence, France

<sup>4</sup>National Research Centre on Human Evolution (CENIEH), Burgos, Spain

<sup>5</sup>Centre for Geographical Studies, IGOT, Universidade de Lisboa, Lisbon, Portugal

<sup>6</sup>Geosciences Barcelona (GEO3BCN-CSIC), Barcelona, Spain

<sup>7</sup>Department of Geography & Centre for Northern Studies, Université Laval, Quebec, Québec, Canada

<sup>8</sup>Consortium: Georges Aumaître, Karim Keddadouche

## Correspondence

Julia Garcia-Oteyza Ciria, Department of Geography, Universitat de Barcelona, Montalegre 6-8, 3r floor, Barcelona 08001, Spain.

Email: [juliagarciadeoteyza@ub.edu](mailto:juliagarciadeoteyza@ub.edu)

## Funding information

Agència de Gestió d'Ajuts Universitaris i de Recerca of the Government of Catalonia; research group ANTALP (Antarctic, Arctic, Alpine Environments; 2017-SGR-1102); Spanish Ministerio de Economía y Competitividad; Spanish Ministry of Science, Innovation and Universities

## Abstract

Although the spatiotemporal oscillations of the Greenland Ice Sheet (GrIS) during the last millennia have played a prominent role in global environmental changes, its glacial response to the natural variability still needs to be better constrained. Here, we focused on the reconstruction of the glacial behavior and deglaciation process along the Tyroler Valley (74° N, 22° E), within the Northeast Greenland National Park. This NW-SE valley connects with the GrIS via the Pasterze Glacier and divides two ice caps (A.P. Olsen Land and Payer Land), this last one feeding two piedmont glaciers (Copeland and Kløft glaciers). For this study, we combined the interpretation of the spatial pattern of geomorphological features and the chronological framework defined by a new dataset of 15 <sup>10</sup>Be cosmic-ray exposure (CRE) ages from glacially polished bedrock surfaces and moraine boulders together with one optically stimulated luminescence (OSL) age of a glaciolacustrine deposit. CRE ages indicate that the deglaciation of the lowest parts of the valley and the exposure of the highest slopes took place during the Early Holocene, at ca. 10–8.5 ka (ka = thousand year [BP]). Furthermore, this ice thinning also favored the disconnection of the valley tributary glaciers. Samples from the moraines of the two tributary glaciers indicate that the deglaciation was not continuous, but it was interrupted by at least three phases of glacial advance during the Neoglacial cooling (before ca. 5.9 ka), and the Little Ice Age

This is an open access article under the terms of the [Creative Commons Attribution-NonCommercial-NoDerivs](https://creativecommons.org/licenses/by-nc-nd/4.0/) License, which permits use and distribution in any medium, provided the original work is properly cited, the use is non-commercial and no modifications or adaptations are made.

© 2023 The Authors. *Land Degradation & Development* published by John Wiley & Sons Ltd.

(LIA, 0.6, and 0.3 ka). The larger piedmont glacier (Copeland Glacier) occupied the valley floor during these major advances, damming the river and allowing the formation of a proglacial glacial lake upvalley, as confirmed by the OSL date of lacustrine sediments that yielded an age of  $0.53 \pm 0.06$  ka. In short, our study provides new evidence of the relative stability of GrIS and the regional ice caps in the area, in which glacial fronts have been rather stable since their advances during the Neoglacial and the LIA.

#### KEYWORDS

cosmic-ray exposure dating, glacial oscillations, Greenland, Holocene, little ice age, Tyroler Valley

## 1 | INTRODUCTION

Spatio-temporal oscillations of the Greenland Ice Sheet (GrIS) have played a prominent role in global environmental changes since the last glacial cycle. At present, the GrIS is a mostly land-based ice mass that stores water equivalent to a ca. 7.2–7.4 m sea level rise (Aschwanden et al. 2019; Bamber et al. 2013), and it is the only Northern Hemisphere ice sheet to have persisted during the last deglacial period. Fluctuations of the ice stored in the GrIS, as well as in the surrounding ice caps and mountain glaciers, promote a large-scale redistributions of oceanic and atmospheric circulation patterns, sea-level changes, redefinition of coastlines, shifts in land cover and ecosystems, and variations in greenhouse gas concentrations (Oliva et al. 2021).

A wide range of terrestrial and marine records from Greenland and the North Atlantic region have shown evidence of abrupt temperature shifts during Termination-1 (T-1; ca. 19–11 ka) that ranged from 5 to 15°C and also featured strong seasonality (Buizert et al. 2014; Vasskog et al. 2015). Such oscillations of the GrIS and other peripheral glaciers during T-1 have been modeled in palaeoglaciological studies (Funder et al. 2011; Vasskog et al. 2015) and have been largely documented based on geomorphological and geochronological data, including the NE sector of Greenland (Biette et al. 2020; Håkansson et al., 2007, 2009, 2011; Kelly et al., 2008; Larsen et al., 2018; Lowell et al., 2013; Skov et al., 2020).

Following T-1, the Northern Hemisphere reached the maximum Holocene insolation in summer (Ressen et al., 2009) and temperatures ca. 2.5°C warmer than present (Axford et al., 2021; Kaufman et al. 2004) were recorded during the Holocene Thermal Maximum (HTM; ca. 10–6 ka; Renssen et al., 2009, 2012). The HTM has been documented in a wide range of paleoenvironmental records in Greenland (Briner et al., 2016; Buizert et al., 2018; Kjær et al., 2022; Vinther et al., 2008; Lusas et al., 2017). Glacier fronts across the GrIS responded to this warm event by receding tens of kilometres within present-day margins during the Early and Mid-Holocene (Kelly et al., 2008). For NE Greenland, most studies suggest an intense deglaciation during late T-1 and the Early Holocene, and since then glaciers have recorded minor advances or retreats depending on the prevailing climate conditions (Adamson et al., 2019; Biette et al., 2020; Garcia-Oteyza et al., 2022).

A cooling trend with relatively high climatic variability occurred in the High Arctic region following the HTM. Although the spatial and temporal patterns of the Holocene glacier advances and retreats are still uncertain, this is particularly true for the Neoglacial time span (starting after ca. 6 ka; Porter & Denton, 1967; McKay et al., 2018; Palacios et al., 2020). The Little Ice Age (LIA; ca. 1300–1850 CE; Grove, 2001) was the last period with documented widespread glacial expansion in NE Greenland (Kjær et al. 2022), as demonstrated by the direct dating of glacial records by means of cosmic-ray exposure (CRE) dating (Biette et al. 2020; Garcia-Oteyza et al. 2022; Jomelli et al. 2022) or even by historical pictures provided by early travellers or hunters that show glaciers larger than those of the present during the late 19th and early 20th centuries in this region (Boyd 1948; Payer 1876).

The deglaciation process at the edges of the Payer Land and A.P. Olsen Land ice caps (NE Greenland) where this research focuses is still poorly understood. Previous research has demonstrated that the major deglaciation took place at the end of T-1 (Garcia-Oteyza et al. 2022). However, knowledge of glacial oscillations during the Holocene is sparser, as studies only report the final deglaciation of the lowest parts of the valleys at ca. 10.5 ka (i.e., Zackenberg; Garcia-Oteyza et al., 2022) with two periods of moraine formation at ca. 11.3 and 10.8 ka and minor Holocene glacial advances at ca. 3.3, 1.2, and 0.4 ka (Clavering Island; Biette et al. 2020; Jomelli et al. 2022).

The objective of this study was to chronologically constrain glacial oscillations in the Tyroler Valley during the Holocene, with a particular focus on the Neoglacial period, to shed light on the prevailing climate regime and environmental response in the region, where this knowledge is still lacking. To this end, we had the following specific objectives:

- To identify landforms generated by glacial oscillations in the Tyroler Valley since the Early Holocene.
- To identify the main phases of glacial expansion and associated environmental implications during the Late Holocene.
- To compare spatio-temporal patterns of neoglacial fluctuations in the Tyroler Valley with those inferred from other regions across Greenland.

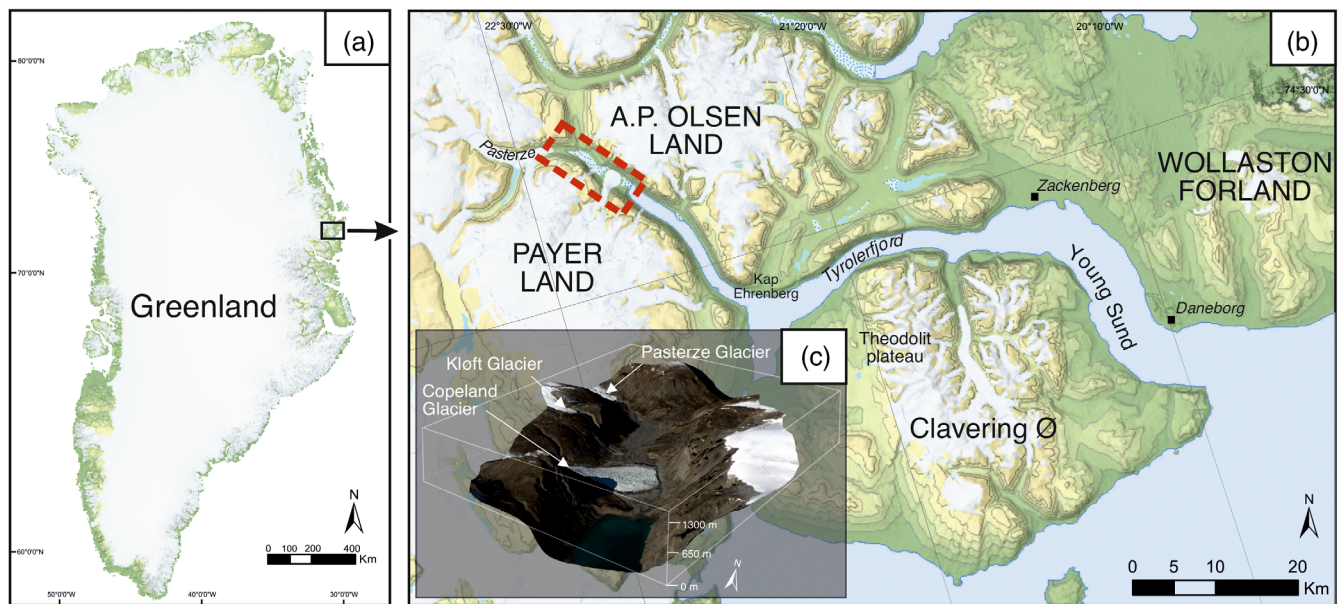


**FIGURE 1** (a) Location of the study area within Greenland; (b) regional setting of the Tyroler Valley, with (c) a 3D representation of the study area. [Colour figure can be viewed at [wileyonlinelibrary.com](https://onlinelibrary.wiley.com/doi/10.1002/ldr.4633)]

## 2 | REGIONAL SETTING

The Tyroler Valley (74° 39' N, 22° 15' W), constitutes an ice-free area forming the unsubmerged continuation of Tyroler Fjord, situated in NE Greenland, within the Northeast Greenland National Park (Figure 1a). The fjord encircles the NW fringe of Clavinging Island and extends inland to the NW between Payer Land and A.P. Olsen Land ice caps. The only human infrastructure in the Tyroler Valley is a hunting hut at the entrance of the valley, which is located ca. 50 km north-west of the Zackenberg Research Station (Figure 1b).

The study area encompasses ca. 10 km NW-SE long and an average width of 1 km, from the mouth of the Tyroler Fjord until the front of the Pasterze Glacier, which drains from the GrIS. Two tributary piedmont glaciers (Kløft and Copeland) descend along the NW slopes of the valley from the Payer Land ice cap and spread across the Tyroler Valley floor, occasionally interrupting the drainage of the river during glacial advances (Figure 1c). The surrounding flat-topped summits rise on either side to between 1000 and 1300 m above sea level (hereafter referred as asl) and connect with steep hillsides descending into the valley. The ice-free areas of the valley floor mainly correspond to an outwash plain, with sediments deposited by a fluvial braided system fed by the Pasterze Glacier meltwater as well as by other proglacial streams. The high sediment load transported by the river has created a delta in contact with the Tyroler Fjord (Figure 1c).

Quaternary sediments cover the valley floor and the lower parts of the hillsides and metamorphic bedrock (Proterozoic orthogneiss and migmatitic sedimentary rocks) is mostly exposed on the upper sections of the slopes (Henriksen & Higgins, 2008). The deglaciated area in Tyroler Valley is underlain by continuous permafrost, probably 200–400 m thick, as observed in nearby Zackenberg Valley (Christiansen et al., 2008; Christoffersen et al., 2008; Hansen et al., 2008).

The study area is characterized by a typical High Arctic polar tundra climate (Kottek et al., 2006). The mean annual air temperature (MAAT) is  $-9.0^{\circ}\text{C}$  at the nearby Zackenberg Research Station, with mean monthly values ranging between  $-19.8^{\circ}\text{C}$  in February and  $6.3^{\circ}\text{C}$  in July (1996–2015 series; Pedersen, 2017). Mean annual precipitation is 367 mm (Pedersen, 2017) that mostly falls as snow, although rain events may occur during the summer months (Hasholt et al., 2008). The fjord remains covered by land-fast sea ice during approximately 9 months per year (Boone et al. 2017). These cold-climate conditions, highly influenced by the East Greenland Current, determine the existence of a High Arctic tundra, with vegetation dominated by dwarf shrub heaths (decreasing in variety and size with elevation), and fell fields on the lower slopes (CAVM Team, 2003).

## 3 | METHODOLOGY

In this study, we combined geomorphological and geochronological approaches – CRE  $^{10}\text{Be}$  and optically stimulated luminescence (OSL) dating, together with historical pictures – to unveil the spatial and temporal patterns of glacial oscillations in the valley. Field work took place in early September 2019, when the snow-free landscape allowed clear identification of geomorphological features as well as the subsequent collection of samples for dating.

### 3.1 | Geomorphological mapping

Prior to field work, to define the sampling strategy, we created a preliminary geomorphological map based on satellite images with a focus on the main glacial landforms as moraines and polished surfaces. This

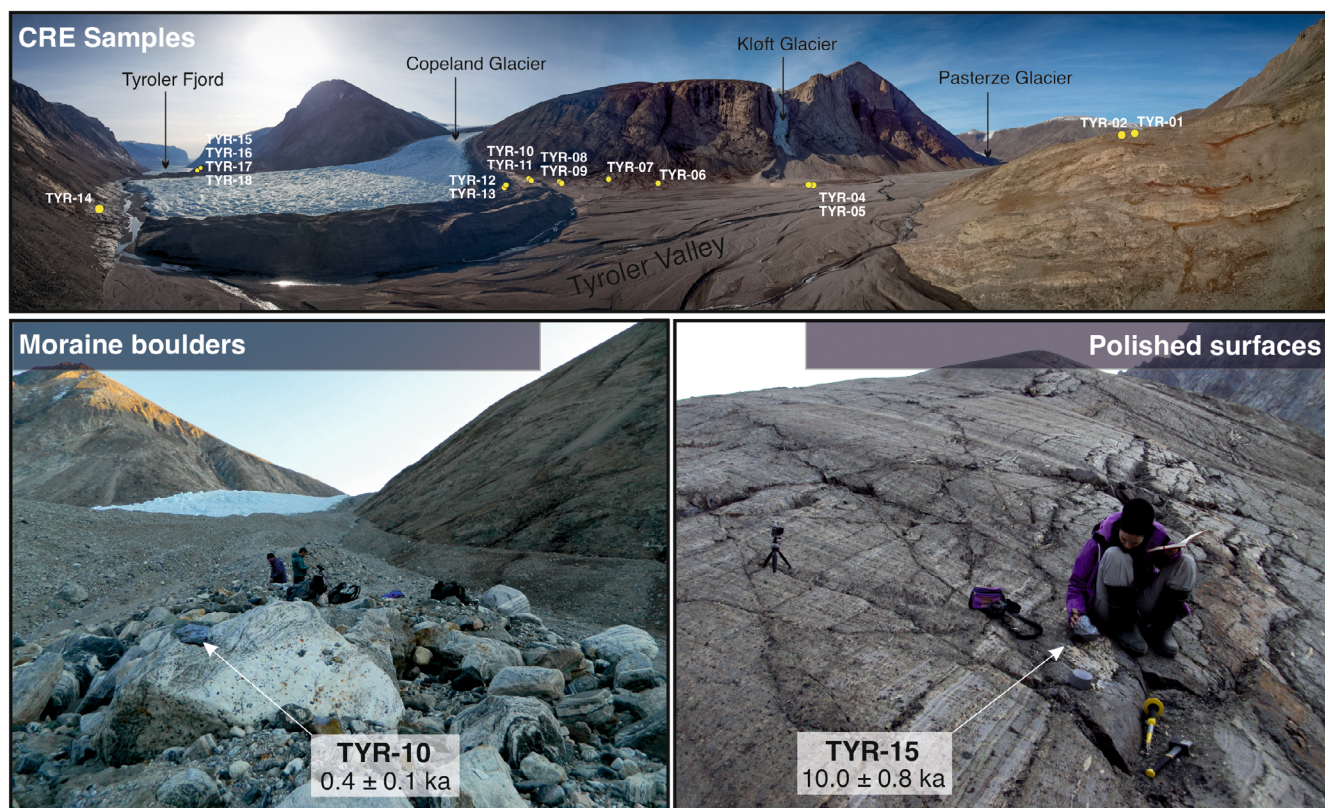


**FIGURE 2** Location of all CRE samples and examples of the different types of glacial features sampled in this study. [Colour figure can be viewed at [wileyonlinelibrary.com](https://onlinelibrary.wiley.com/doi/10.1002/ldr.4633)]

map was validated based on in-situ observations and included newly observed landforms. The final geomorphological map was drawn by outlining the landforms in the ARCMAP 10.8 work environment over an orthorectified panchromatic satellite SPOT-6/7 (1.5 m resolution) image from 08-19-2017 and the digital surface model ArcticDEM (2 m spatial resolution) provided by Porter et al. (2018).

### 3.2 | Sample collection

Considering the geomorphological map and field observations, we collected 18 samples for  $^{10}\text{Be}$  CRE dating from two types of glacial features (Figure 2): moraine boulders (11 samples) and polished bedrock surfaces (7 samples). For each sample, we took approximately 1 kg of the rock's most surficial layer ( $\leq 5$  cm thick) using a hammer and chisel and recorded the main field data: geomorphological unit, geographical coordinates, elevation, and the measurements for the subsequent geometric correction of the topographic shielding by the surrounding relief. Field data and sample attributes are listed in Table 1.

In addition, we also collected two samples for OSL dating from an alluvial fan deposit upstream of the Copeland Glacier front (Figure 3). Samples were collected from the upper, middle, and lower parts of this 20-m thick sedimentary deposit composed of fine gravels and coarse sands. To avoid sunlight exposure when collecting the samples, we used a light-proof (opaque) core tube of dark PVC (4 cm diameter).

### 3.3 | CRE laboratory analytical procedures and age calculation

Sample crushing and sieving (0.25–1 mm fraction) were carried out at the Laboratory of Physical Geography of the Universidad Complutense de Madrid, Spain. Further physical and chemical procedures were conducted at the Laboratoire National des Nucleides Cosmogéniques ( $\text{LN}_2\text{C}$ ) of the Centre Européen de Recherche et d'Enseignement des Géosciences de l'Environnement (CEREGE, Aix-en-Provence, France).

Laboratory procedures followed the same protocol and guidelines of our previous work in the area as described in Garcia-Oteyza et al. (2022). A small change in the procedure was made before performing the magnetic separation, with a first leaching of a mixture of hydrochloric (HCl), hexafluorosilicic ( $\text{H}_2\text{SiF}_6$ ) and hydrofluoric (HF) acids, in order to facilitate the quartz isolation process and to start the physical separation of quartz/non-quartz minerals with a more concentrated sample. The measurement of the  $^{10}\text{Be}/^9\text{Be}$  ratios on the BeO targets were performed at the French 5 MV 'Accélérateur pour les Sciences de la Terre, Environnement et Risques' (ASTER) the facility at CEREGE, using the same calibrations and standards previously described in Garcia-Oteyza et al. (2022). Some samples yielded relatively high uncertainties (TYR-02, TYR-06) due to low current values, and one provided a non-valid measurement (TYR-03) and were thus considered chemical outliers and discarded

**TABLE 1** Sample locations, topographic shielding factor, and sample thickness.

Sample ID	Landform	Latitude (dd)	Longitude (dd)	Elevation (m asl)	Topographic shielding factor (dimensionless)	Thickness (cm)
<i>Upper valley roche moutonnée</i>						
TYR-01	Polished surface	74.6415	-22.1791	280	0.9938	2
TYR-02	Polished surface	74.6372	-22.1815	241	-	4
<i>Kløft Glacier external moraine</i>						
TYR-03	Lateral moraine	74.6336	-22.2080	136	-	4
TYR-04	Lateral moraine	74.6335	-22.2080	134	0.9807	4
TYR-05	Lateral moraine	74.6329	-22.2088	134	0.9807	4
<i>Middle valley polished surface</i>						
TYR-06	Polished surface	74.6298	-22.2123	135	-	3.8
TYR-07	Polished surface	74.6254	-22.2018	153	0.9872	2.5
<i>Copeland Glacier</i>						
<i>External moraine</i>						
TYR-08	Lateral moraine	74.6232	-22.1987	164	0.9873	3
TYR-09	Lateral moraine	74.6231	-22.1987	164	0.9873	3.2
<i>Middle moraine</i>						
TYR-10	Lateral moraine	74.6234	-22.1913	172	0.9871	3.4
TYR-11	Lateral moraine	74.6233	-22.1914	170	0.9871	3.5
<i>Internal moraine</i>						
TYR-12	Lateral moraine	74.6264	-22.1815	129	0.9699	3.5
TYR-13	Lateral moraine	74.6264	-22.1813	131	0.9699	2.7
<i>Frontal Copeland polished surface</i>						
TYR-14	Polished surface	74.6294	-22.14685	45	0.9754	2.0
<i>Fjord entrance_upper roche moutonnée</i>						
TYR-15	Polished surface	74.6053	-22.1043	150	0.9890	5.0
<i>Fjord entrance moraine</i>						
TYR-16	Lateral moraine	74.6059	-22.1068	120	0.9813	5
TYR-17	Lateral moraine	74.6059	-22.1070	120	0.9813	3.5
<i>Fjord entrance_lower roche moutonnée</i>						
TYR-18	Polished surface	74.6066	-22.1060	100	0.9779	5

Note: Highlighted in italics: samples with a non-valid AMS measurement, considered chemical outliers and discarded for exposure age calculations and discussion.

for further exposure age calculations and discussion. All analytical data are shown in Table 2.

Exposure ages were calculated with the CRONUS-Earth online calculator, version 3.0 (Balco et al., 2008; <https://hess.ess.washington.edu/>), with the Arctic-wide sea-level/high-latitude  $^{10}\text{Be}$  production rate ( $3.96 \pm 0.15 \text{ atoms g}^{-1} \text{ yr}^{-1}$ ) (Young et al. 2013) and the “Lm” (Lal/Stone) time-dependent scaling model (Lal 1991; Stone 2000). For all samples, a  $2.7 \text{ g cm}^{-3}$  density was assumed, and no corrections of erosion or snow shielding were applied and the partial shielding effect of the surrounding topography was corrected for all sampling sites using the Topographic Shielding Calculator

version 2 ([http://stoneage.ice-d.org/math/skyline/skyline\\_in.html](http://stoneage.ice-d.org/math/skyline/skyline_in.html)) (Table 2).

### 3.4 | OSL laboratory analytical procedures

The two collected samples for OSL dating were treated at the luminescence laboratory of the National Research Centre on Human Evolution (CENIEH, Burgos, Spain), under controlled light conditions to extract quartz grains of 90–250  $\mu\text{m}$  size. These were used for OSL measurements to estimate the burial dose. Luminescence

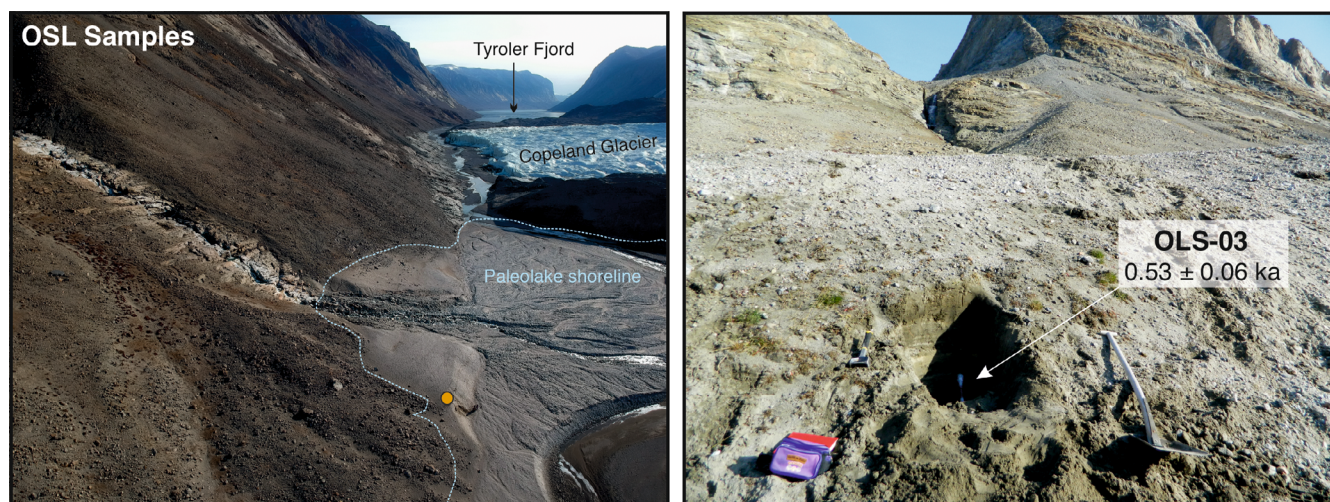


**FIGURE 3** Location and picture of the OSL sample site. [Colour figure can be viewed at [wileyonlinelibrary.com](https://onlinelibrary.wiley.com/doi/10.1002/ldr.4633)]

measurements were carried out in a Risø OSL/TL reader (TL-DA 20) equipped with a built-in beta source.

The radionuclide activities measured by high-resolution gamma spectrometry (Table 3) at the Radioisotopes Unit of the University of Sevilla were used to calculate the annual dose rate by applying conversion factors from (Guérin et al., 2011). The contribution from cosmic rays was calculated according to Prescott and Hutton (1994) and attenuation caused by water content was taken into account. Total annual dose rates were determined using ‘DRAC’ (dose rate and age calculator, Durcan et al., 2015) and are summarized in Table 4.

The luminescence signal from sample TYROSL –2 was dim and the poor signal-to-noise ratio did not allow the estimation of an equivalent dose. In contrast, quartz multi-grain aliquots of sample TYROSL–3 showed a well-defined luminescence signal, and despite showing a slow decay, the dose recovery test indicated that a given dose could be recovered within 1-sigma. The dose distribution derived from the measurement of 48 aliquots was normally distributed (Figure 4). The population of the dose was reduced by excluding outliers (values outside 1.5-times the interquartile range) from the estimation of the equivalent dose which was done applying the central age model (CAM; Galbraith et al. 1999). The estimated burial dose and derived age are summarized in Table 4.

### 3.5 | Historical data

The Tyroler Fjord area is the site of an extensive scientific and non-scientific exploration history framed within the first European expeditions in NE Greenland carried out during the 19th and first half of the 20th centuries (Rule et al. 2005). The texts and pictures provided in those early surveys included descriptions of the landforms and processes in the region. Two expeditions in particular described in detail the features in the Tyroler Valley, particularly the glaciers: The Second German North Pole expedition of 1869–70 led by Karl Koldewey (Payer 1876) and the Louise A. Boyd's Arctic expedition of 1937

(Boyd 1948). The comparison of the data in these documents with the present-day glacier fronts allowed us to establish the magnitude of ice recession since the end of the LIA.

## 4 | RESULTS

### 4.1 | Geomorphological setting

The Tyroler Valley is a U-shaped glacial valley that is mostly deglaciated, but is also occupied by one large piedmont glacier (Copeland Glacier) that covers a large portion of the lower valley floor. The valley is surrounded by several ice caps on its NE (A.P. Olsen Land) and SW (Payer Land) fringes, and connects with the GrIS via the Pasterze Glacier at the western end of the valley (Figure 5). Current glaciers display a clear asymmetry between the opposite slopes of the valley, with well-developed ice tongues forming piedmont glaciers on NE slopes fed by the ice sheet that caps the Payer Land, and much shorter or almost non-existent tongues on the steep NW slopes descending from the A.P. Olsen Land ice cap. The Copeland Glacier (Figure 5) is currently the only glacier reaching the valley bottom, where it has generated a complex moraine system with several ridges surrounding the margins and with its front at present being ca. 100 m away from the opposite hillside (left slope) of the valley. This tongue descends from the Payer Land Ice Cap through a steep and narrow valley for ca. 5 km, and it is on average 700 m wide. Field work allowed the identification of a wide range of Tyroler Valley geomorphological landforms.

The terminal lobe of the piedmont glacier (ca.  $2 \times 1.5$  km and  $3.5$  km<sup>2</sup>) is surrounded on both sides by similarly shaped moraine complexes with their outer flanks standing 30 to 50 m above the outwash plain and with a maximum slope of 35°. The lobe's front consists of a 15 m (on average) high ice cliff with a calving base washed out by the river. The Kløft Glacier (Figure 5) echoes its larger neighbor in source and distance from it but does not reach the valley bottom at

**TABLE 2** AMS analytical data and calculated exposure ages.

Sample name	Quartz weight (g)	Mass of carrier ( $^{9}\text{Be}$ mg)	$^{10}\text{Be}/^{9}\text{Be}$ ( $10^{-14}$ )	Blank correction (%)	$[^{10}\text{Be}]$ ( $10^4$ atoms $\text{g}^{-1}$ ) $\pm 1\sigma$ (atoms $\text{g}^{-1}$ )	$^{10}\text{Be}$ age (ka) <sup>a</sup>	Internal uncertainty (ka)	External uncertainty (ka)
<i>Upper valley roche moutonnée</i>								
TYR-01	43.6794	0.44135	7.805 $\pm 0.402$	2.91	5.116 $\pm$ 0.273	9.2	0.6	0.5
<i>Kløft Glacier external moraine—Arithmetic mean age: 0.3 <math>\pm</math> 0.2 ka (n = 2)</i>								
TYR-04	33.0422	0.44259	0.371 $\pm 0.044$	62.51	0.125 $\pm$ 0.049	0.3	0.1	0.1
TYR-05	32.0741	0.44307	0.375 $\pm 0.077$	60.30	0.138 $\pm$ 0.08	0.3	0.2	0.2
<i>Middle valley polished surface</i>								
TYR-07	37.1995	0.15035	5.553 $\pm 0.216$	3.51	4.537 $\pm$ 0.178	9.3	0.4	0.5
<i>Copeland Glacier</i>								
<i>External moraine</i>								
TYR-08	40.6263	0.45290	1.034 $\pm 0.06$	21.92	0.602 $\pm$ 0.05	1.3	0.1	0.1
TYR-09	38.4679	0.45284	8.537 $\pm 0.266$	2.66	6.537 $\pm$ 0.211	13.8	0.4	0.7
<i>Middle moraine—Arithmetic mean age: 0.6 <math>\pm</math> 0.2 ka (n = 2)</i>								
TYR-10	40.2721	0.44740	0.486 $\pm 0.056$	46.17	0.194 $\pm$ 0.052	0.4	0.1	0.1
TYR-11	35.7175	0.44368	0.656 $\pm 0.063$	34.46	0.357 $\pm$ 0.062	0.7	0.1	0.1
<i>Internal moraine—Arithmetic mean age: 0.3 <math>\pm</math> 0.2 ka (n = 2)</i>								
TYR-12	35.7226	0.44861	0.366 $\pm 0.035$	62.58	0.115 $\pm$ 0.04	0.3	0.1	0.1
TYR-13	36.1246	0.44927	0.318 $\pm 0.038$	71.97	0.074 $\pm$ 0.041	0.2	0.1	0.1
<i>Frontal Copeland polished surface</i>								
TYR-14	30.7325	0.44870	3.144 $\pm 0.117$	7.28	2.844 $\pm$ 0.119	5.9	0.2	0.3
<i>Fjord entrance_upper roche moutonnée</i>								
TYR-15	14.9181	0.44915	2.728 $\pm 0.195$	8.38	5.029 $\pm$ 0.398	10.0	0.8	0.9
<i>Fjord entrance moraine</i>								
TYR-16	22.7161	0.45045	3.156 $\pm 0.12$	6.23	3.921 $\pm$ 0.164	8.3	0.3	0.5
TYR-17	40.5580	0.44973	49.44 $\pm 1.535$	0.46	36.464 $\pm$ 1.138	77.4	2.5	3.8
<i>Fjord entrance_lower roche moutonnée</i>								
TYR-18	31.2899	0.45021	4.245 $\pm 0.155$	4.64	3.892 $\pm$ 0.152	8.4	0.3	0.5
<b>Chemistry blank details<sup>b</sup></b>								
Blank name	Mass of carrier ( $^{9}\text{Be}$ mg)		$^{10}\text{Be}/^{9}\text{Be}$ ( $10^{-14}$ )		$[^{10}\text{Be}]$ ( $10^4$ atoms)			
BK1	0.45088		0.222 $\pm$ 0.04		6.703 $\pm$ 1.219			
BK2	0.44576		0.23 $\pm$ 0.032		6.862 $\pm$ 0.964			
BK3	0.45242		0.196 $\pm$ 0.028		5.921 $\pm$ 0.832			

Note:  $^{10}\text{Be}/^{9}\text{Be}$  ratios were inferred from measurements at the ASTER AMS facility. No correction of erosion and snow cover have been made.

<sup>a</sup> $^{10}\text{Be}$  ages assuming a density of 2.7  $\text{g cm}^{-3}$  and a zero-erosion scenario.

<sup>b</sup>In parallel to the sample treatment, four blanks were prepared: BK1 (processed with samples TYR-01, TYR-05, TYR-06, TYR-10, and TYR-11), BK2 (processed with samples TYR-02, TYR-04, TYR-08, TYR-09, TYR-12, TYR-13, TYR, 13, TYR-14, TYR-15, and TYR-17), and BK3 (processed with samples TYR-07, TYR-16, and TYR-18).



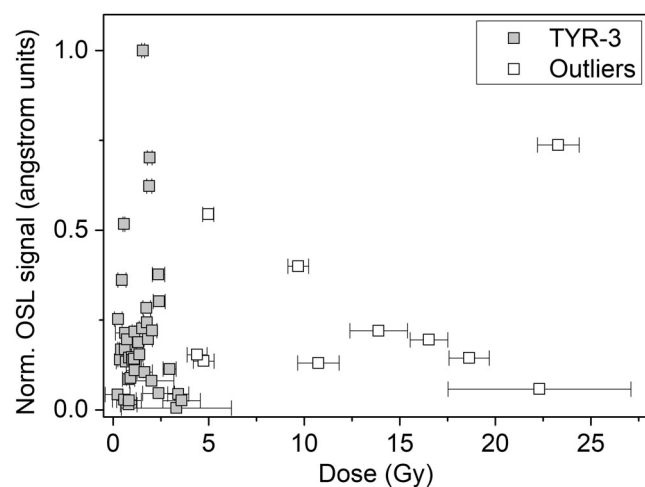
**TABLE 3** Radionuclide activity concentration.

Sample	Lab (US) code	Depth (m)	Moisture (%)	$^{40}\text{K}$ (Bq/kg $^{-1}$ )	$^{232}\text{Th}$ (Bq/kg $^{-1}$ )	$^{238}\text{U}$ (Bq/kg $^{-1}$ )
TYROSL-2	4198	0.4	20	613 ± 25	27.4 ± 1.1	12.3 ± 0.5
TYROSL-3	4199	0.7	20	519 ± 23	33.5 ± 1.3	22.3 ± 1.3

Note: Also shows the depth used to calculate the contribution of cosmic rays to the total dose rate and the moisture. A 5% error have been added to the moisture values.

**TABLE 4** Summary of total dose rates for the two samples, estimated burial dose and corresponding age of sample TYR-3 for which OSL measurements were possible.

Sample	Dose rate (Gy/ka)	Burial dose (Gy)	Age (ka)
TYROSL-2	2.44 ± 0.11	X ± X	X ± X
TYROSL-3	2.42 ± 0.11	1.3 ± 0.1	0.53 ± 0.06

**FIGURE 4** Dose distribution derived from the OSL measurement of sample TYR-3. Open icons indicate the identified outliers excluded from the age estimation. The normalized natural OSL signal is plotted as a function of the measured dose and corresponding uncertainty for each individual aliquot.

present. It also descends from the plateau through a deep, narrow gorge that is ca. 1 km long, and is 100 m wide on average. At present, the glacier front remains hanging at the lower-middle part of the slope at ca. 600 m from the external moraine system mapped and ca. 300 m from the internal moraine system.

Finally, at the head of the valley, the Pasterze Glacier flows between steep slopes and there is a frontal moraine 200 m from the current glacier terminus. A large proglacial outwash plain, reshaped by the braided fluvial system, extends from the terminus of the Pasterze Glacier to the external moraines created by the Copeland and Kløft glaciers (Figure 5). In some places along the margins of this plain, glacio-lacustrine sequences of fine-grained sediments have accumulated due to the damming of the valley by the advance of glaciers descending from the slopes.

A wide range of glacial, periglacial, and alluvial landforms is also found on the slopes surrounding the valley floor, with two main domains. Slopes above ~400 m a.s.l. have exposed bedrock and are affected by very intense periglacial conditions (i.e., with the presence of permafrost and frost heave): This setting includes flat-topped summits (at ca. 1000 m asl), mostly covered by ice caps and their outlet tongues. These plateaus connect with the Tyroler Valley through steep slopes (30° on average), where hanging valleys and scarps can be found. On slopes below ~400 m asl, erosive and depositional glacial landforms are widespread, including glacially polished bedrock surfaces, lateral moraine systems and erratic boulders. In some cases, these glacial features are partially covered by debris slopes, talus cones, and alluvial fans, particularly on the lower sections of the slopes.

The existence of polished bedrock surfaces at between 40 and 300 m above the valley floor is indicative of the ice thickness reached by the glacier in the past. In past glacial phases, the area must have been occupied by a single glacial tongue formed by the coalescence of the Pasterze Glacier and other tributaries descending from both the Payer Land and A.P. Olsen Land ice caps. Next to the fjord, at the lowest part of the valley, there is a *roche moutonnée* (ca. 150 m high) that was sampled for CRE dating to establish the onset of deglaciation of the Tyroler Valley. In this sector, we collected four samples: one from the highest exposed bedrock surfaces ca. 150 m a.s.l. (TYR-15), another from the lower part of the bedrock ca. 100 m a.s.l. (TYR-18), and two from scattered moraine boulders in the middle part of the slope ca. 120 m a.s.l. (TYR-16 and TYR-17). This moraine located at the entrance of the valley from the fjord represents the most distal remnants of a lateral moraine stretching along the valley's slopes, with no signs of reworking on its right hillside (Figure 5).

We also took two samples from a *roche moutonnée* located on the left valley side, upstream of the Copeland Glacier, to reconstruct the glacier's past recession and thinning: one near the culmination of the bedrock surface (TYR-1) and the other ca. 40 m lower (TYR-2). On the other side of the valley, between Copeland and Kløft glaciers, two polished and striated gneiss surfaces at the foot of the slope were targeted (TYR-6 and TYR-7) to determine the time of individualization of these two glaciers.

The valley also includes geomorphic evidence of potentially recent glacial oscillations near the termini of the Copeland and Kløft glaciers. The former created a complex moraine system, with two main polygenic lateral moraines on the southern side and up to five ridges on the northern margin of the glacier, where we focused the sampling strategy: (i) Two samples were taken from the most external ridge (TYR-8 and TYR-9), which shows stable slopes as suggested by

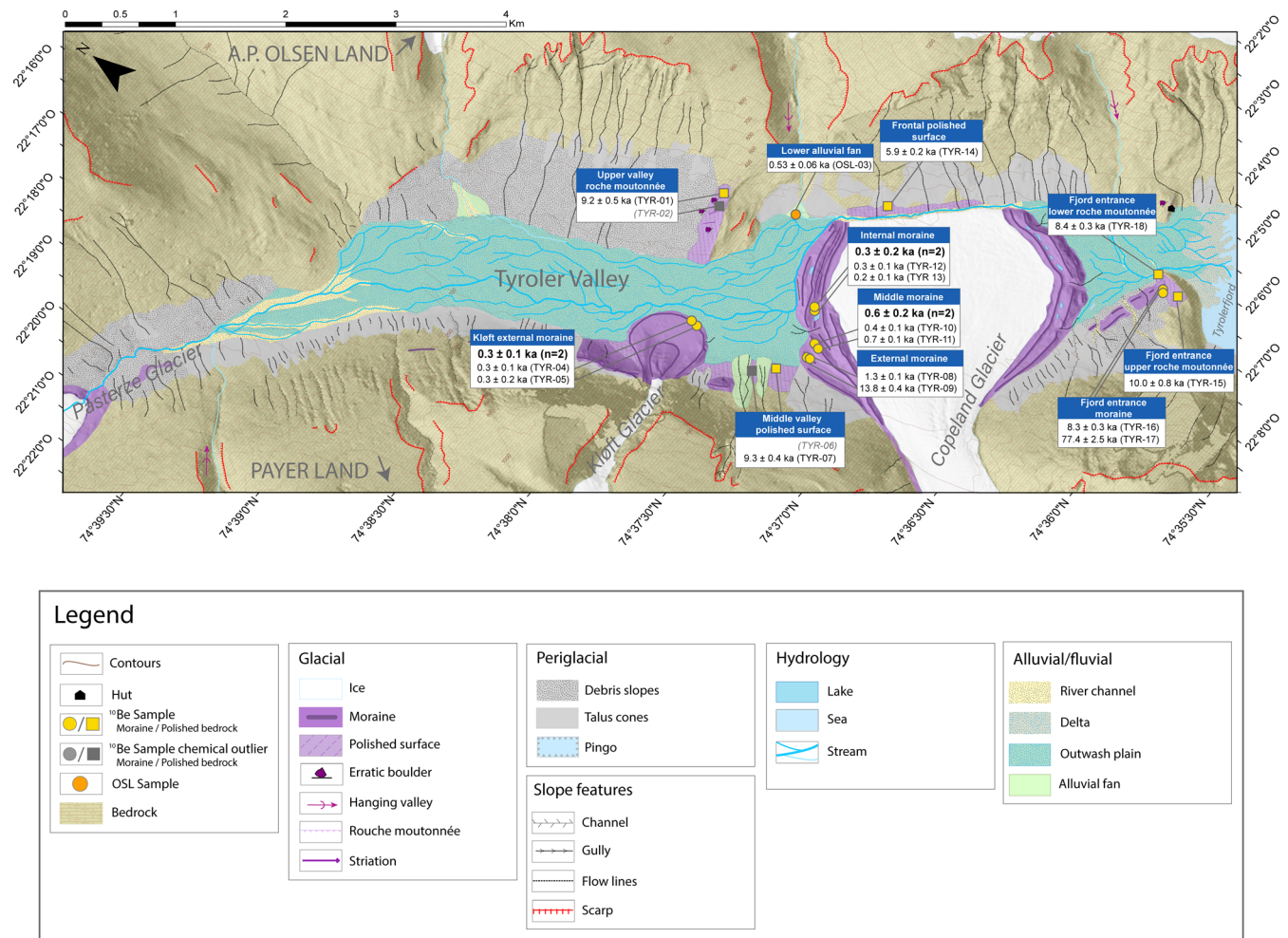


**FIGURE 5** Geomorphological map including the main landforms together with the CRE and OSL results. [Colour figure can be viewed at [wileyonlinelibrary.com](http://wileyonlinelibrary.com)]

the presence of mosses; (ii) Two more samples (TYR-10 and TYR-11) were taken from the middle and more voluminous unvegetated ridge; and (iii) two further samples (TYR-12 and TYR-13) were obtained from an internal moraine crest. The two moraine ridges next to the glacier were ice-cored features and were thus not sampled to avoid unexpected ages associated with ongoing stabilization as the inner ice core melts. These lateral moraines do not extend over the frontal part of the glacier, which is very close to the opposite slope. The existence of polished and striated bedrock devoid of unconsolidated sediments on the lower part of the slope (from the riverbed level to 50 m above it) in front of the Copeland Glacier terminus reveals the occurrence of past periods of glacial expansion. One sample (TYR-14) was obtained from this polished surface. Past phases of glacier expansion favored the formation and evolution of glacier-dammed lakes. River drainage must have been blocked in the past due to the expansion of the Copeland Glacier across to the opposite valley slope, causing the formation of a proglacial lake extending over much of the present-day outwash plain fed by the meltwater stream from the Pasterze Glacier and other tributaries. This lake's level would have fluctuated depending on the

glacier volume blocking the valley. Its last maximum advance favored the development of its maximum paleo-shoreline level of ca. 151 m above the present-day valley bottom. This paleo-shoreline is widely continuous along the valley and is defined by horizontal layers of fine-grained silt and clay-sized sediments, although in some areas it has been eroded or disturbed by streams and mass wasting processes. Indeed, lateral streams formed alluvial fans upon contact with the hypothesized paleolake that must have been frozen several months per year. This is the case of the alluvial fan formed by the stream draining the Olsen Land ice cap on the NW edge of the Copeland Glacier (Figure 3) that is composed of two terraces of fine-grained sediments (mostly sands and small gravels). Two samples were taken for OSL dating of the middle (TYROSL -02) and lower (TYROSL -03) parts of the deposit.

The two moraine systems of the Kjøft Glacier extend across the valley floor, with the external moraines being of greater size than the inner ones and showing evidence of the piedmont character of the glacier when they were formed. We collected three samples from the external frontal moraine arch to establish the phase of its maximum

expansion (TYR-3, TYR-4, and TYR-5). The inner arched moraine complex is located at the foot of the slope, with a 5-m high frontal moraine arch; inside, the area is filled with fine-grained sediments deposited by an active alluvial fan from the meltwater stream of the Kløft Glacier.

## 4.2 | Geochronological data

The location and the chronological data of the samples are presented in Figure 5. CRE results show evidence of the occurrence of past periods during the Holocene with larger glacial systems than today. The lower area of the Tyroler Valley was deglaciated during the Early Holocene, as indicated by samples from the highest surfaces of the *roche moutonnée* aged  $10.0 \pm 0.8$  ka (TYR-15) and the lower surface at  $8.4 \pm 0.3$  ka (TYR-18). Two boulders of the moraine constrained between these surfaces yielded exposure ages of  $8.3 \pm 0.3$  ka (TYR-16) and  $77.4 \pm 2.5$  ka (TYR-17) respectively. The sample collected from the *roche moutonnée* located in the middle part of the valley yielded an exposure age of  $9.2 \pm 0.6$  ka (TYR-01), and of the two samples taken from polished surfaces between the Kløft and Copeland glaciers, only one returned a valid age of  $9.3 \pm 0.4$  ka (TYR-07).

The sample obtained from the polished surface on the slope opposite the Copeland Glacier returned an exposure age of  $5.9 \pm 0.2$  ka (TYR-14). In general, more recent ages were obtained from boulders of the Copeland Glacier moraine system: (i) two boulders from the external moraine ridge returned ages of  $1.3 \pm 0.1$  ka (TYR-08) and  $13.8 \pm 0.4$  ka (TYR-09); (ii) two boulders from the middle moraine ridge yielded ages of  $0.4 \pm 0.1$  ka (TYR-10) and  $0.7 \pm 0.1$  ka (TYR-11) with a mean age of  $0.6 \pm 0.2$  ka; and (iii) two moraine boulders of the inner ridge reported ages of  $0.3 \pm 0.1$  ka (TYR-12) and  $0.2 \pm 0.1$  ka (TYR-13), with a mean age of  $0.3 \pm 0.2$  ka (Figure 5).

The samples collected from the external moraines of the Kløft Glacier were aged  $0.3 \pm 0.1$  ka (TYR-04) and  $0.3 \pm 0.2$  ka (TYR-05), with a mean of  $0.3 \pm 0.2$  ka. Finally, the only available OSL age estimated from the samples taken from the glacio-lacustrine deposit on the left side of the valley gave an age of  $0.53 \pm 0.06$  ka (TYROSL-03).

## 5 | DISCUSSION

The combined interpretation of the spatial pattern of geomorphological features and the chronological framework defined by CRE and OSL ages enabled the reconstruction of the spatio-temporal glacial oscillations in the Tyroler Valley.

### 5.1 | Considerations on the geochronology dataset prior to interpretation

Some CRE ages must be interpreted with caution as, apparently, they do not follow the expected chronostratigraphical sequence. TYR-09

( $13.8 \pm 0.4$  ka), collected from the external lateral moraine ridge of the Copeland Glacier, had a much older exposure age than the other boulder of the same moraine system (TYR-10). Although this moraine ridge seemed geomorphologically stable, the CRE age may indicate nuclide inheritance in this boulder, probably associated with insufficient reworking given the proximity of the moraine to the upper sections of exposed bedrock that supply debris to the glacier. TYR-17 ( $77.4 \pm 2.5$  ka), from a moraine boulder at the valley entrance, also returned a much older exposure age than expected relative to the ages obtained in the valley. The moraine's age as constrained by two samples of the exposed bedrock surface from the upper and lower parts of the *roche moutonnée* (TYR-15,  $10.0 \pm 0.8$  ka; TYR-18,  $8.4 \pm 0.3$  ka) fits reasonably well with the other sample collected from this landform (TYR-16;  $8.3 \pm 0.3$  ka). The moraine ridge was defined by dispersed boulders forming a line on a relatively horizontal step of the exposed bedrock; while the subrounded morphology of the TYR-17 boulder suggests that it was efficiently reworked during englacial transport, its CRE age indicated that the boulder retained an inheritance signal from past deglacial phases. The horizontal plateau surfaces of the ice caps must favor the existence of cold-based glaciers with reduced erosion capacity, which may also help explain the occurrence of nuclide concentrations inherited from previous exposure phases. As such, these two samples were not considered when establishing the geomorphological evolution in this valley, which thus includes 13  $^{10}\text{Be}$  CRE samples of Holocene age ranging from  $10.0 \pm 0.8$  (TYR-15) to  $0.2 \pm 0.1$  ka (TYR-13) (Figure 6).

### 5.2 | Deglaciation chronology

The oldest moraine (TYR-16) as well as the glacially polished surfaces distributed across the valley were of Early-Middle Holocene age. The remaining ages, from moraine boulder samples, were of Late Holocene age (Figure 7). Based on the geomorphological and geochronological evidence, we identify three major glacial phases in Tyroler Valley during the Holocene:

#### 1. Glacial occupation of the valley

The presence of glacially polished surfaces from ca. 300 m above the valley floor demonstrates that the area was heavily glaciated during the last glacial cycle (Figure 7). The entire valley was probably filled by ice to the mountain tops, similar to what occurred in neighbouring valleys tens of km beyond the current glacier fronts where ice thicknesses reached ca. 800 m asl (Garcia-Oteyza et al., 2022). The expansion of the GrIS as well as of the surrounding ice caps during the last glacial cycle has been already documented in several regions of NE Greenland. Prior to the Last Glacial Maximum (LGM), between 115–75 ka glacier fronts reached the inner shelf (Funder et al., 2011; Lecavalier et al. 2014). The Tyroler Valley must therefore have been occupied by one large glacial system fed by several tributaries descending from the GrIS, as well as from the Payer Land and A.P. Olsen Land ice caps, which were connected at that time.

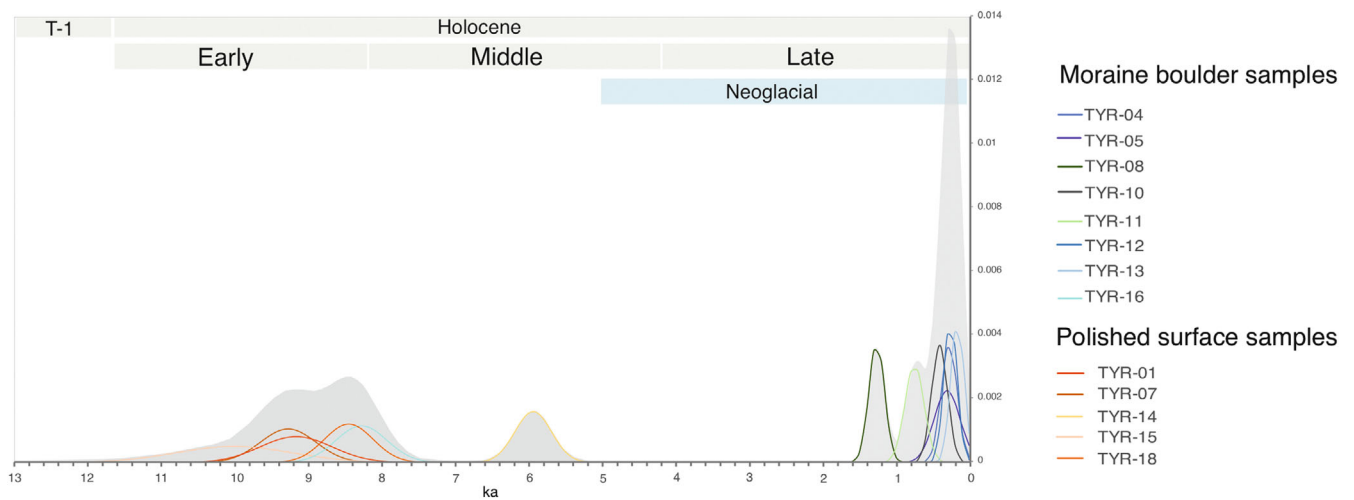


**FIGURE 6** Probability distribution functions of  $^{10}\text{Be}$  ages with (with external uncertainties) for all the samples of our final accepted age dataset (TYR-09 and TYR-17 were not considered). [Colour figure can be viewed at [wileyonlinelibrary.com](http://wileyonlinelibrary.com)]

## 2. Glacial recession and individualization of ice masses

As temperatures rose more than  $20^{\circ}\text{C}$  in central Greenland during T-1 (Buizert et al. 2018), the glaciers present in Tyroler Valley receded and thinned significantly. As a result, some tributaries disconnected from the main ice stream extending over much of the Tyroler Fjord, as occurred in Zackenberg Valley at 11–10 ka (Garcia-Oteyza et al., 2022) and on the Theodolit plateau (Clavering Island) after ca. 10 ka (Biette et al., 2020). The lowlands of the Tyroler Valley also became ice-free at ca. 10–8.5 ka as suggested by the polished surfaces at the entrance of the valley ( $10.0 \pm 0.8$ – $8.4 \pm 0.3$  ka) as well as upstream from the Copeland Glacier ( $9.2 \pm 0.5$  ka). Indeed, sample TYR-07 indicates that ice thinning favored the disconnection of the Copeland and Kløft glaciers, which occurred at  $9.3 \pm 0.4$  ka. The Early Holocene deglaciation was not continuous, and long-term glacial shrinking was interrupted by at least one period of minor glacier advance or standstill as indicated by the formation of valley side moraines, and by the remnants of moraines of the same phase identified at the upper part of the roche moutonnée ( $8.3 \pm 0.3$  ka) (Figure 7). The thinning glaciers progressively exposed the upper slopes of the valley, where paraglacial dynamics started to operate, and shrinking glaciers were supplied with sediments that accumulated on the lower mountain slopes, forming alluvial fans, talus cones, and debris slopes. Since ca. 9–8.5 ka, only two (piedmont) glaciers persisted on the NE side of the valley (Kløft and Copeland), expanding or retreating in response to prevailing climate conditions.

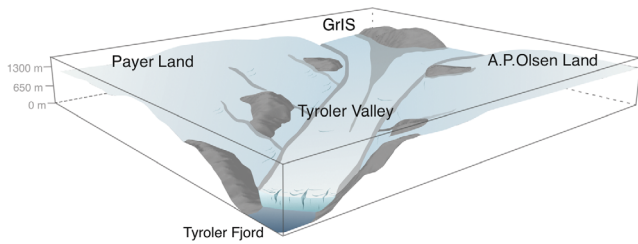
## 3. Neoglacial and LIA advances

No geomorphic evidence of glacial activity is preserved from the Middle Holocene, between ca. 8 and 6 ka. The only CRE age obtained from the polished bedrock located on the opposite slope of the Copeland Glacier front indicated that a Holocene glacial advance was followed by a retreat at  $5.9 \pm 0.2$  ka. Further CRE ages are needed to

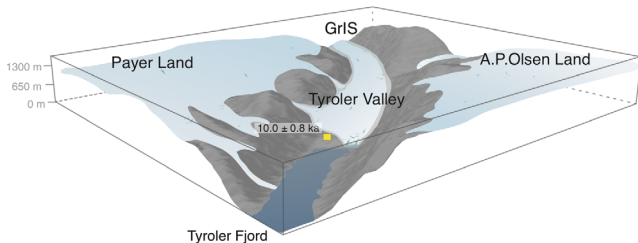
confirm that this glacial advance corresponded to the onset of the neoglacial in the region. Any glacial advances during the last millennia must have been of reduced scope, as suggested by the moraine systems generated by the Copeland and Kløft glaciers that extend between ca. 700 and 100 m from present-day fronts. Whereas the most external moraine of the Copeland Glacier suggests a phase of glacial expansion during the Dark Ages Cold Period (DACP; ca. AD 400–765; Helama et al., 2017) at ca. 1.3 ka – as also reported by Biette et al. (2020) in the neighboring Clavering Island –, the rest of the multiple moraine ridges of these piedmont glaciers reported ages spanning different phases of the LIA, with two major glacial advances at ca. 0.6 ka and 0.3 ka. During these major advances Copeland Glacier occupied the valley floor, damming the river and causing the formation of a proglacial glacial lake, as confirmed by the accumulation of the fine-grained sediments of the alluvial fan aged  $0.53 \pm 0.06$  ka (Figure 7). Glacial retreat after the last LIA advance at ca. 0.3 ka must have favored the drainage of the paleolake. Since that time, glacier fronts fluctuated within limits defined by the dated internal moraines. This pattern of pulses of retreat and advance resulting from post-LIA climatic shifts also been reported in other (sub)Arctic small debris-free glaciers (Fernández-Fernández et al. 2017).

The comparison of the current situation in the valley with pictures from historical expeditions (Figure 8) shows evidence of the glacier retreat in the valley since 1869 CE, when glaciers were much more extensive (Payer 1876). Descriptions and sketches of the valley entrance show an ice barrier close to the fjord and five glacier tributaries descending from the plateaus and feeding the main valley glacier (two glacial tributaries from the A.P Olsen Land, Kløft, Copeland and Pasterze glacial tongues). Pictures taken in 1937 CE during the expedition led by Louise A. Boyd (Boyd 1948) show the position of the Copeland Glacier front, tens of metres beyond its current front. Moreover, the river has washed away the frontal moraine that existed in these pictures (Figure 8). However,

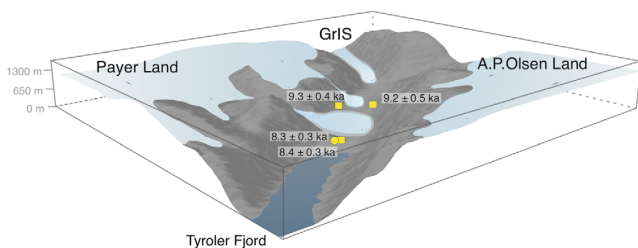
## 1. Glacial occupation of the valley



## 2a. Glacial recession (ca. 10 ka)



## 2b. Individualization of the ice masses (ca. 10-8.5 ka)



## 3. Neoglacial and LIA advances

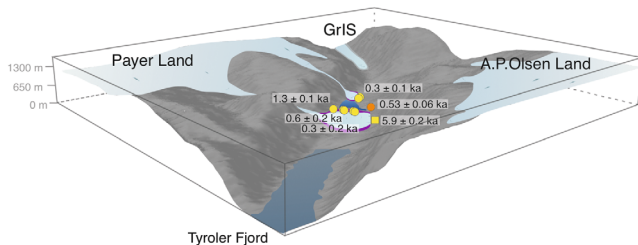


**FIGURE 7** Idealized reconstruction model for the glacial evolution of Tyroler Valley and the proposed glacial phases. Base map obtained from the current Digital Elevation Model (Porter et al. 2018). [Colour figure can be viewed at [wileyonlinelibrary.com](http://wileyonlinelibrary.com)]

the most considerable change is found in the Kløft Glacier, which reached the bottom of the valley in 1937 CE, forming a terminal lobe surrounded by the outermost moraine (Figure 8). Indeed, Google Earth Pro satellite images ranging from 1984 until 2015 (Google Earth Pro 7.3.4.8642 (1984–2015), 74°37′31.99″N, 22°10′03.48″, elevation 70 m, LANDSAT/COPERNICUS, [Online]. Available at <https://www.google.com/earth/>) show that the front of the Kløft Glacier still formed a lobe in the valley floor inside the inner moraines until ca. 2010, when it began to recede upslope.

## 5.3 | Glacial oscillations in NE Greenland since termination 1

Holocene climate variability and glacial evolution of Greenland shows complex and diverse spatio-temporal patterns (Briner et al., 2016; Young et al. 2020). Following the temperature evolution reconstructed from the NGRIP 1 and 2 ice cores (Walker et al., 2018), we identify the following phases regarding the glacial evolution in the Tyroler Valley:

## 5.3.1 | Early Holocene (11.7 to 8.2 ka; Greenlandian)

The maximum Holocene summer insolation in the Northern Hemisphere during the Early Holocene led to the highest summer temperatures (Buizert et al., 2018), initiating the HTM (Renssen et al., 2009). The timing and intensity of the HTM in Greenland show high regional variability, promoting a widespread trend of glacial retreat of both the GriS and mountain glaciers and ice caps (Axford et al. 2021), only interrupted by short periods of glacial stabilization in some regions (Young et al., 2020). Glacial response in S and W Greenland during the HTM was more diffuse than in the N and E sectors of the island, where the prevailing warmer temperatures promoted a strong glacier retreat during the Early Holocene (Briner et al. 2016).

In summary, broadly across Greenland, the GriS had already retreated behind present-day boundaries by 10–9 ka and the retreat continued, except during the 8.2 ka cold event (Carlson et al., 2014; Larsen et al., 2015; Reusche et al., 2018; Skov et al. 2020). The valley lowlands of our study area became ice-free and the different tributaries disconnected from the main glacier at ca. 10–8.5 ka, which correlated with the GriS long-term glacial shrinking during the HTM. One of our samples also shows the interruption of this trend, reporting a minor glacial advance or stillstand with moraine formation at ca. 8.3 ka, which might be associated with the cold peak that occurred at 8.2 ka (Figure 9).

## 5.3.2 | Middle Holocene (8.2 to 4.3 ka; Northgrippian)

Orbital-induced reduced summer insolation in the Northern Hemisphere promoted a gradual cooling trend in Greenland from 8.2 ka onwards (McKay et al. 2018). Superimposed on this long-term trend, changes in the strength of the Atlantic Meridional Overturning Circulation and other regional forcing mechanisms affected glacial dynamics: ice masses of the North Atlantic region generally retreated significantly during the mid-Holocene and re-advanced in the late Holocene (Jomelli et al. 2022). Summer temperatures fell until 1–1.5 °C below present-day temperatures by the end of the mid-Holocene, albeit with a high degree of variability across Greenland (Lasher and Axford 2019). Consequently, glaciers began to re-advance in what has been called the neoglaciation (Porter 2000). However, as the end



**FIGURE 8** Sketch and photographs from historical expeditions (Boyd 1948; Payer 1876) that visited the area compared with modern pictures from the same areas. [Colour figure can be viewed at [wileyonlinelibrary.com](https://onlinelibrary.wiley.com/doi/10.1002/lid.4633)]

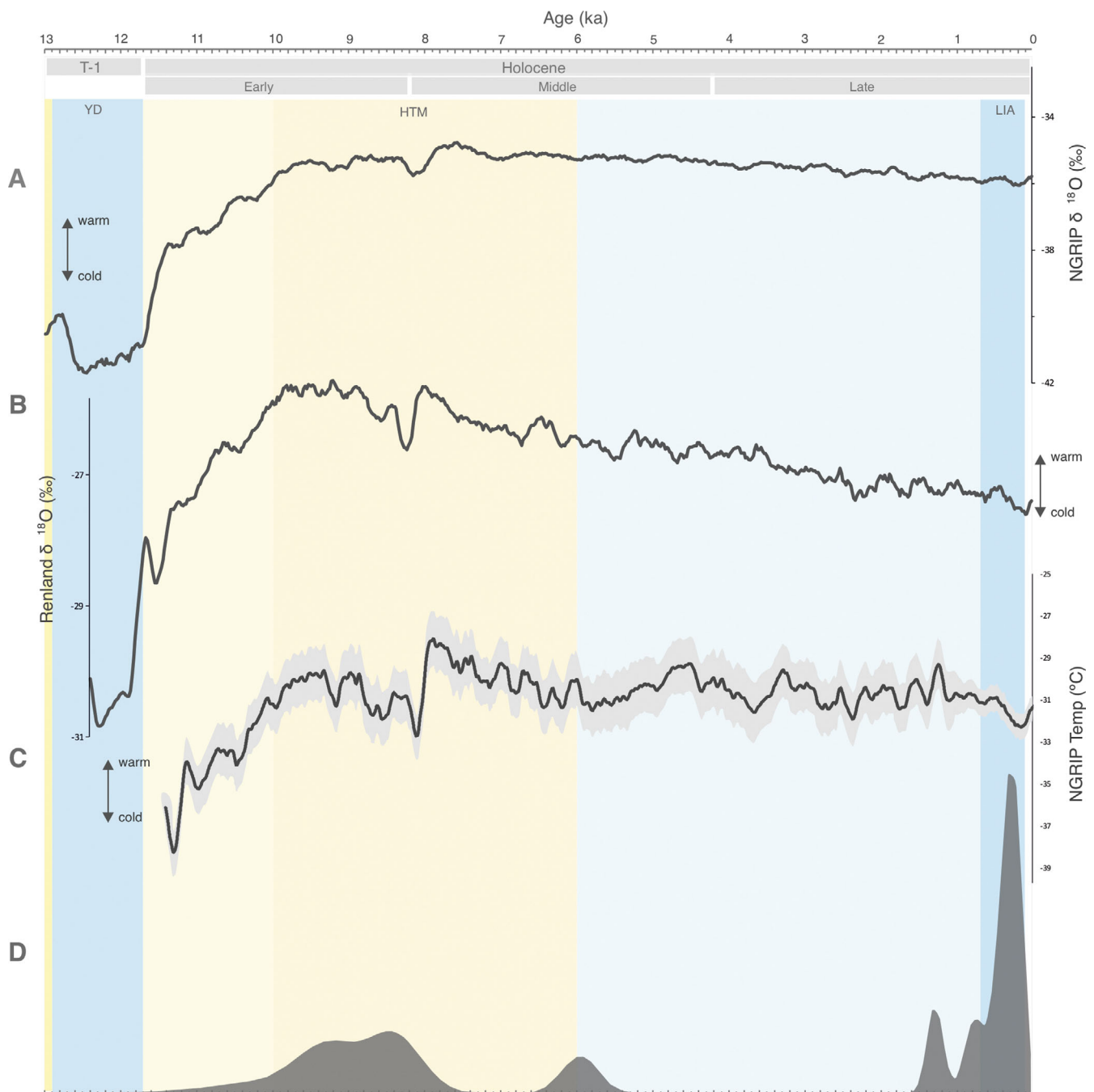


**FIGURE 9** (a)  $\delta^{18}\text{O}$  record of the NGRIP ice core smoothed with 15 interval moving average (GICC05modelext, 5-point running mean; Rasmussen et al. (2006)). (b)  $\delta^{18}\text{O}$  record of the ice core from Renland Ice Cap in eastern Greenland with 10 interval moving average (GICC05 timescale) (Vinther et al. 2008). (c) NGRIP ice core reconstructed temperature from argon and nitrogen isotopes ( $^{15}\text{N}$  -  $^{40}\text{Ar}$ ), with  $2\sigma$  error bands (gray shading) and 150 interval moving average (Kobashi et al. 2017). (d) Probability distribution functions of our final dataset of exposure ages. [Colour figure can be viewed at [wileyonlinelibrary.com](http://wileyonlinelibrary.com)]

of the HTM was time-transgressive across the island, the beginnings of glacial advances show great regional, even local, variability.

The GrIS reached its global minimum Holocene extent at 7 ka, but the retreat of some of its fronts was delayed until 4–3 ka, or even later (Larocca et al., 2020a,b; Larsen et al., 2018; Schweinsberg et al., 2019). Local mountain glaciers and ice caps recorded a similar response pattern to the GrIS to changing Holocene climate trends. In

S Greenland most of the glaciers disappeared between 7.1 and 5.5 ka and began to recover from 3.1 ka to 1.3 ka onwards (Larocca et al., 2020a; Jomelli et al. 2022). In SW Greenland, some glaciers survived throughout the HTM and began to recover from 4.3 ka onwards (Larocca et al., 2020b). In E Greenland, the Renland Ice Cap was smaller than present by 9.5 ka and began to recover at 4 ka (Medford et al., 2021).

In NE Greenland, the Tyroler Valley lacks extensive geomorphic evidence of glacial activity for the Middle Holocene, as was also reported in other studies in the region (Biette et al. 2022). We only detected a phase of glacial advance prior to ca. 5.9 ka that may be associated with the onset of neoglaciation in the area (Figure 9). Since that time, and until ca. 1.3 ka, climate conditions must not have been conducive to periods of major glacial expansion in the valley. It should be noted, however, that the proximity of the glacier front to the opposite hillside hinders the preservation of glacial landforms that may have been deposited during that phase.

### 5.3.3 | Late Holocene (4.3 ka to present; Meghalayan)

The most widespread neoglacial advances in Greenland can be grouped into three main periods: at 2.5–1.7 ka, 1.2–0.9 ka, and 1250–1900 CE (Kjær et al., 2022), albeit with a significant regional variability. In W Greenland, glaciers advanced and exceeded their present-day limits at 3.7, 2.8, 1.5 ka, and during the LIA at 1400 and 1700 CE (Schweinsberg et al., 2019). In Inglefield Land, NW Greenland, glaciers remained behind current boundaries from 5.8 ka until the beginning of the LIA at 1450 CE (Søndergaard et al., 2020). The northern GrlS margin also showed a relative stability during the Late Holocene, with only two neoglacial advances of similar magnitude detected at 2.8 ka and 1650 CE (Reusche et al., 2018). In E Greenland, the Renland Ice Cap exceeded the present limits by 3.3 ka, 1.3 ka, and 1 ka, advancing similarly during the LIA (Medford et al., 2021), and the Bregne Ice Cap in Scoresby Sund recorded the maximum glacial expansion during the LIA at ca. 0.74 ka (Levy et al., 2014).

In NE Greenland, glacial advances were dated in Clavering Island at ca. 3 ka, 1.2 ka, and 0.5 ka based on CRE on moraine boulders (Biette et al. 2020). The analysis of proglacial lake sediments near the Zackenberg Valley (Figure 1) revealed the occurrence of three neoglacial advances over the last two millennia (Adamson et al., 2019): one occurred at 1.3–1.2 ka during the Dark Ages Cold Period, a second advance took place at ca. 0.8 ka during the Medieval Climate Anomaly, and the last one was associated with the onset of the LIA that showed a smaller advance than the previous ones and peaked at 1250–1400 CE (Adamson et al., 2019). Our records from the Tyroler Valley also showed three main glacial advances for the Late Holocene at ca. 1.3, 0.6 and 0.3 ka, broadly synchronous with previous glacial chronologies as well as with ice core temperature reconstructions in Greenland (Figure 9).

## 6 | CONCLUSIONS

This study introduces new geomorphological and geochronological data of glacial oscillations in Tyroler Valley, NE Greenland, during the Holocene. Scientific knowledge about the response of glaciers to changing temperature and moisture regimes in Greenland during the present-day interglacial is still incipient. As in other areas in NE Greenland, CRE ages indicate that the deglaciation of the lowest parts of the valley, as well as the exposure of the highest slopes, took place

during the Early Holocene, at ca. 10–8.5 ka. Our data reveal that the GrlS and surrounding ice caps in the area only expanded during neoglacial advances and the LIA. Prior to this historical phase, the Copeland Glacier recorded two periods of glacial growth before ca. 5.9 ka and at ca. 1.3 ka. Subsequently, both the Copeland and Kløft glaciers expanded during the LIA forming moraines ca. 100–700 m from present-day glacier fronts. Two periods of moraine formation were detected in Copeland Glacier at ca. 0.6 and 0.3 ka, while only one at ca. 0.3 ka was detected for the Kløft Glacier. The expansion of the Copeland Glacier during the LIA dammed Tyroler Valley and caused the formation of a large proglacial lake, as confirmed by glaciolacustrine sediments OSL dated ca. 0.53 ka. Since the last major LIA advance, glacial fronts have oscillated as demonstrated by historical images but have remained relatively close to the LIA moraines.

In summary, our data expands and strengthens the chronology of Holocene glacial oscillations in Greenland, in particular its NE sector where no previous studies have precisely constrained neoglacial oscillations. Future studies should elucidate whether the chronology of glacial culminations and retreats in the Tyroler Valley over the Mid-Late Holocene represents a local response to prevailing climate conditions or formed part of a more general pattern that occurred across the High Arctic region.

### ACKNOWLEDGMENTS

This study was funded by the NEOGREEN (PID2020-113798GB-C31) and PALEOGREEN (CTM2017-87976-P) projects of the Spanish Ministerio de Economía y Competitividad. Field research was also supported by the research group ANTALP (Antarctic, Arctic, Alpine Environments; 2017-SGR-1102) funded by the Agència de Gestió d'Ajuts Universitaris i de Recerca of the Government of Catalonia. Julia Garcia-Oteyza was supported by an FPI fellowship from the Spanish Ministry of Science, Innovation and Universities, and Marcelo Fernandes by a PhD fellowship of the Fundação para a Ciência e Tecnologia of Portugal (UIDB/00295/2020). The  $^{10}\text{Be}$  measurements were performed at the ASTER AMS national facility (CEREGE, Aix-en-Provence), which is supported by the INSU/CNRS and the ANR through the “Projets thématiques d'excellence” programme for the “Equipements d'excellence” ASTER-CEREGE action and IRD. We are also grateful to Jesús Ruiz and Zackenberg Research Station for field support.

### DATA AVAILABILITY STATEMENT

All data used in this study are available upon request from the authors.

### ORCID

Julia Garcia-Oteyza Ciria  <https://orcid.org/0000-0002-0187-2922>

Marc Oliva  <https://orcid.org/0000-0001-6521-6388>

David Palacios  <https://orcid.org/0000-0002-8289-0398>

### REFERENCES

- Adamson, K., Lane, T., Carney, M., Bishop, T., & Delaney, C. (2019). High-resolution proglacial lake records of pre-Little Ice Age glacier advance, Northeast Greenland. *Boreas*, 48(3), 535–550. <https://doi.org/10.1111/bor.12361>



- Aschwanden, A., Fahnestock, M. A., Truffer, M., Brinkerhoff, D. J., Hock, R., Khroulev, C., Mottram, R., & Abbas Khan, S. (2019). Contribution of the Greenland Ice Sheet to sea level over the next millennium. *Science Advances*, 5(6), eaav9396. <https://doi.org/10.1126/sciadv.aav9396>
- Axford, Y., De Vernal, A., & Osterberg, E. C. (2021). Past warmth and its impacts during the Holocene thermal maximum in Greenland. *Annual Review of Earth and Planetary Sciences*, 49, 279–307. <https://doi.org/10.1146/annurev-earth-081420-063858>
- Balco, G., Stone, J. O., Lifton, N. A., & Dunai, T. J. (2008). A complete and easily accessible means of calculating surface exposure ages or erosion rates from  $^{10}\text{Be}$  and  $^{26}\text{Al}$  measurements. *Quaternary Geochronology*, 3(3), 174–195. <https://doi.org/10.1016/j.quageo.2007.12.001>
- Bamber, J. L., Griggs, J. A., Hurkmans, R. T. W. L., Dowdeswell, J. A., Gogineni, S. P., Howat, I., Mouginot, J., Paden, J., Palmer, S., Rignot, E., & Steinhage, D. (2013). A new bed elevation dataset for Greenland. *The Cryosphere*, 7(2), 499–510. <https://doi.org/10.5194/tc-7-499-2013>
- Biette, M., Jomelli, V., Chenet, M., Braucher, R., Menviel, L., Swingedouw, D., Rinterknecht, V., & ASTERTeam. (2022). Evidence of the largest Late Holocene mountain glacier extent in southern and southeastern Greenland during the middle Neoglacial from  $^{10}\text{Be}$  moraine dating. *Boreas*, 51, 61–77. <https://doi.org/10.1111/bor.12555> ISSN 0300-9483.
- Biette, M., Jomelli, V., Chenet, M., Braucher, R., Rinterknecht, V., Lane, T., & Aster Team. (2020). Mountain glacier fluctuations during the Lateglacial and Holocene on Clavering Island (northeastern Greenland) from  $^{10}\text{Be}$  moraine dating. *Boreas*, 49, 873–885. <https://doi.org/10.1111/bor.12460>
- Boone, W., Rysgaard, S., Kirillov, S., Dmitrenko, I., Bendtsen, J., Mortensen, J., Meire, L., Petrusevich, V., & Barber, D. G. (2017). Circulation and fjord-shelf exchange during the ice-covered period in Young Sound-Tyrolerfjord, Northeast Greenland (74° N). *Estuarine, Coastal and Shelf Science*, 194, 205–216. <https://doi.org/10.1016/j.ecss.2017.06.021>
- Boyd, L. A. (1948). *The coast of Northeast Greenland: With hydrographic studies in the Greenland Sea. The Louise a. Boyd Arctic expeditions of 1937 and 1938*. American Geographical Society.
- Briner, J. P., McKay, N. P., Axford, Y., Bennike, O., Bradley, R. S., Vernal, A. D., Fisher, D., Francus, P., Fréchette, B., Gajewski, K., Jennings, A., Kaufman, D. S., Miller, G., Rouston, C., & Wagner, B. (2016). Holocene climate change in Arctic Canada and Greenland. *Quaternary Science Reviews*, 147, 340e364. <https://doi.org/10.1016/j.quascirev.2016.02.010>
- Buizert, C., Gkinis, V., Severinghaus, J. P., He, F., Lecavalier, B. S., Kindler, P., Leuenberger, M., Carlson, A. E., Vinther, B., Masson-Delmotte, V., White, J. W. C., Liu, Z., Otto-Bliesner, B., & Brook, E. J. (2014). Greenland temperature response to climate forcing during the last deglaciation. *Science*, 345(6201), 1177–1180. <https://doi.org/10.1126/science.1254961>
- Buizert, C., Keisling, B. A., Box, J. E., He, F., Carlson, A. E., Sinclair, G., & DeConto, R. M. (2018). Greenland-wide seasonal temperatures during the last deglaciation. *Geophysical Research Letters*, 45(4), 1905–1914. <https://doi.org/10.1002/2017GL075601>
- Carlson, A. E., Winsor, K., Ullman, D. J., Brook, E. J., Rood, D. H., Axford, Y., LeGrande, A. N., Anslow, F. S., & Sinclair, G. (2014). Earliest Holocene south Greenland ice sheet retreat within its late Holocene extent. *Geophysical Research Letters*, 41, 5514–5521. <https://doi.org/10.1002/2014GL060800>
- CAVM Team. (2003). Circumpolar Arctic Vegetation Map. (1:7,500,000 scale), Conservation of Arctic Flora and Fauna (CAFF) Map No. 1. US Fish Wildl. Serv. AK. <https://www.Geobot.uaf.edu/cavm/>[Verified 1 August 15 July 2015] 2.
- Christiansen, H. H., Sigsgaard, C., Humlum, O., Rasch, M., & Hansen, B. U. (2008). Permafrost and periglacial geomorphology at Zackenberg. *Advances in Ecological Research*, 40, 151–174. ISSN 0065-2504, ISBN 9780123736659. [https://doi.org/10.1016/S00652504\(07\)00007-4](https://doi.org/10.1016/S00652504(07)00007-4), <https://www.sciencedirect.com/science/article/pii/S0065250407000074>
- Christoffersen, K. S., Amsinck, S. L., Landkildehus, F., Lauridsen, T. L., & Jeppesen, E. (2008). Lake flora and fauna in relation to ice-melt, water temperature and chemistry at Zackenberg. *Advances in Ecological Research*, 40, 371–389. ISSN 0065-2504, ISBN 9780123736659. [https://doi.org/10.1016/S00652504\(07\)00016-5](https://doi.org/10.1016/S00652504(07)00016-5)
- Durcan, J. A., King, G. E., & Duller, G. A. T. (2015). DRAC: Dose rate and age calculator for trapped charge dating. *Quaternary Geochronology*, 28 (January 2013), 54–61. <https://doi.org/10.1016/j.quageo.2015.03.012>
- Fernández-Fernández, J. M., Andrés, N., Sæmundsson, Þ., Brynjólfsson, S., & Palacios, D. (2017). High sensitivity of North Iceland (Tröllaskagi) debris-free glaciers to climatic change from the ‘little ice age’ to the present. *Holocene*, 27(8), 1187–1200. <https://doi.org/10.1177/0959683616683262>
- Funder, S., Kjeldsen, K. K., Kjær, K. H., & Cofaigh, C. O. (2011). The Greenland ice sheet during the past 300,000 years: A review. *Developments in Quaternary Science*, 15, 699–713. <https://doi.org/10.1016/j.quascirev.2011.07.022>
- Galbraith, R. F., Roberts, R. G., Laslett, G. M., Yoshida, H., & Olley, J. M. (1999). Optical dating of single and multiple grains of quartz from Jinmium rock shelter, northern Australia: Part I, experimental design and statistical models. *Archaeometry*, 41(2), 339–364. <https://doi.org/10.1111/j.1475-4754.1999.tb00987.x>
- García-Oteyza, J., Oliva, M., Palacios, D., Fernández-Fernández, J. M., Schimmelpennig, I., Andrés, N., Antoniadou, D., Christiansen, H. H., Humlum, O., Léanni, L., Jomelli, V., Ruiz-Fernández, J., Rinterknecht, V., Lane, T. P., Adamson, K., Aumaitre, G., Bourlès, D., & Keddadouche, K. (2022). Late glacial deglaciation of the Zackenberg area, NE Greenland. *Geomorphology*, 401, 108125. <https://doi.org/10.1016/j.geomorph.2022.108125>
- Grove, J. M. (2001). The Initiation of the ‘Little Ice Age’ in Regions Round the North Atlantic. *Climatic Change*, 48, 53–82. <https://doi.org/10.1023/A:1005662822136>
- Guérin, G., Mercier, N., & Adamiec, G. (2011). Dose-Rate Conversion Factors: Update Dose-Rate Conversion Factors: Update. *Ancient TL*, 29(1), 5–8.
- Håkansson, L., Alexanderson, H., Hjort, C., Möller, P., Briner, J. P., & Possnert, A. A. (2009). Late Pleistocene glacial history of Jameson Land, Central East Greenland, derived from cosmogenic  $^{10}\text{Be}$  and  $^{26}\text{Al}$  exposure dating. *Boreas*, 38(2), 244–260. <http://dx.doi.org/10.1111/j.1502-3885.2008.00064.x>
- Håkansson, L., Briner, J. P., Aldahan, A., & Possnert, G. (2011).  $^{10}\text{Be}$  data from meltwater channels suggest that Jameson Land, East Greenland, was ice-covered during the last glacial maximum. *Quaternary Research*, 76(3), 452–459. <https://doi.org/10.1016/j.yqres.2011.06.007>
- Håkansson, L., Graf, A., Strasky, S., Ivy-Ochs, S., Kubik, P. W., Hjort, C., & Schlüchter, C. (2007). Cosmogenic  $^{10}\text{Be}$ -ages from the store Koldewey Island, NE Greenland. *Geografiska Annaler, Series A: Physical Geography*, 89(3), 195–202. <http://www.jstor.org/stable/4621510>
- Hansen, B. U., Sigsgaard, C., Rasmussen, L., Cappelen, J., Hinkler, J., Mernild, S. H., Petersen, D., Tamstorf, M. P., Rasch, M., & Hasholt, B. (2008). Present-day climate at Zackenberg. *Advances in Ecological Research*, 40, 111–149. ISSN 0065-2504 ISBN 9780123736659. [https://doi.org/10.1016/S0065-2504\(07\)00006-2](https://doi.org/10.1016/S0065-2504(07)00006-2), <https://www.sciencedirect.com/science/article/pii/S0065250407000062>
- Hasholt, B., Mernild, S. H., Sigsgaard, C., Elberling, B., Petersen, D., Jakobsen, B. H., Hansen, B. U., Hinkler, J., & Søgaard, H. (2008). Hydrology and transport of sediment and solutes at Zackenberg. *Advances in Ecological Research*, 40, 197–221. Academic Press ISSN 0065-2504. ISBN 9780123736659. <https://doi.org/10.1016/>

- S00652504(07)00009-8, <https://www.sciencedirect.com/science/article/pii/S0065250407000098>
- Helama, S., Jones, P. D., & Briffa, K. R. (2017). Dark Ages cold period: A literature review and directions for future research. *Holocene*, 27, 1600–1606. <https://doi.org/10.1177/0959683617693898>
- Henriksen, N., & Higgins, A. (2009). Descriptive text to Geological map of Greenland, 1:500 000, Dove Bugt, Sheet 10. *Geological Survey of Denmark and Greenland Map Series*, 4, 1–32 <https://doi.org/10.34194/geusm.v4.4581>.
- Jomelli, V., Swingedouw, D., Vuille, M., Favier, V., Goehring, B., Shakun, J., Braucher, R., Schimmelpfennig, I., Menviel, L., Rabatel, A., Martin, L. C. P., Blard, P. H., Condom, T., Lupker, M., Christl, M., He, Z., Verfaillie, D., Gorin, A., Aumaitre, G., ... Keddadouche, K. (2022). In-phase millennial-scale glacier changes in the tropics and North Atlantic regions during the Holocene. *Nature Communications*, 13(1), 1–12. <https://doi.org/10.1038/s41467-022-28939-9>
- Kaufman, D. S., Ager, T. A., Anderson, N. J., Anderson, P. M., Andrews, J. T., Bartlein, P. J., Brubaker, L. B., Coats, L. L., Cwynar, L. C., Duvall, M. L., Dyke, A. S., Edwards, M. E., Eisner, W. R., Gajewski, K., Geirsdóttir, A., Hu, F. S., Jennings, A. E., Kaplan, M. R., Kerwin, M. W., ... Wolfe, B. B. (2004). Holocene thermal maximum in the Western Arctic (0–180° W). *Quaternary Science Reviews*, 23(5–6), 529–560. <https://doi.org/10.1016/j.quascirev.2003.09.007>
- Kelly, M. A., Lowell, T. V., Hall, B. L., Schaefer, J. M., Finkel, R. C., Goehring, B. M., Alley, R. B., & Denton, G. H. (2008). A 10Be chronology of Lateglacial and Holocene Mountain glaciation in the Scoresby Sund region, East Greenland: Implications for seasonality during Lateglacial time. *Quaternary Science Reviews*, 27(25–26), 2273–2282. <https://doi.org/10.1016/j.quascirev.2008.08.004>
- Kjær, K. H., Bjørk, A. A., Kjeldsen, K. K., Hansen, E. S., Andresen, C. S., Siggaard-Andersen, M. L., Khan, S. A., Søndergaard, A. S., Colgan, W., Schomacker, A., Woodroffe, S., Funder, S., Rouillard, A., Jensen, J. F., & Larsen, N. K. (2022). Glacier response to the little ice age during the neoglacial cooling in Greenland. *Earth-Science Reviews*, 227(March). <https://doi.org/10.1016/j.earscirev.2022.103984>
- Kobashi, T., Menviel, L., Jeltsch-Thömmes, A., Vinther, B. M., Box, J. E., Muscheler, R., Nakaegawa, T., Pfister, P. L., Döring, M., Leuenberger, M., Wanner, H., & Ohmura, A. (2017). Volcanic influence on centennial to millennial Holocene Greenland temperature change. *Scientific Reports*, 7(1), 1441. <https://doi.org/10.1038/s41598-017-01451-7>
- Lal, D. (1991). Cosmic ray labeling of erosion surfaces: In situ nuclide production rates and erosion models. *Earth and Planetary Science Letters*, 104(2–4), 424–439. [https://doi.org/10.1016/0012-821X\(91\)90220-C](https://doi.org/10.1016/0012-821X(91)90220-C)
- Larocca, L. J., Axford, Y., Bjørk, A. A., Lasher, G. E., & Brooks, J. P. (2020a). Local glaciers record delayed peak Holocene warmth in South Greenland. *Quaternary Science Reviews*, 241, 106421. <https://doi.org/10.1016/j.quascirev.2020.106421>
- Larocca, L. J., Axford, Y., Woodroffe, S. A., Lasher, G. E., & Gawin, B. (2020b). Holocene glacier and ice cap fluctuations in southwest Greenland inferred from two lake records. *Quaternary Science Reviews*, 246, 106529. <https://doi.org/10.1016/j.quascirev.2020.106529>
- Larsen, N. K., Kjær, K. H., Lecavalier, B., Bjørk, A. A., Colding, S., Huybrechts, P., ... Olsen, J. (2015). The response of the southern Greenland ice sheet to the Holocene thermal maximum. *Geology*, 43(4), 291–294.
- Larsen, N. K., Levy, L. B., Carlson, A. E., Buizert, C., Olsen, J., Strunk, A., Bjørk, A. A., & Skov, D. S. (2018). Instability of the Northeast Greenland ice stream over the last 45,000 years. *Nature Communications*, 9(1), 1–8. <https://doi.org/10.1038/s41467-018-04312-7>
- Lasher, G. E., & Axford, Y. (2019). Medieval warmth confirmed at the Norse Eastern Settlement in Greenland. *Geology*. <https://doi.org/10.1130/g45833.1>
- Lecavalier, B. S., Milne, G. A., Simpson, M. J. R., Wake, L., Huybrechts, P., Tarasov, L., Kjeldsen, K. K., Funder, S., Long, A. J., Woodroffe, S., Dyke, A. S., & Larsen, N. K. (2014). A model of Greenland ice sheet deglaciation constrained by observations of relative sea level and ice extent. *Quaternary Science Reviews*, 102, 54–84. <https://doi.org/10.1016/j.quascirev.2014.07.018>
- Levy, L. B., Kelly, M. A., Lowell, T. V., Hall, B. L., Hempel, L. A., Honsaker, W. M., ... Axford, Y. L. (2014). Holocene fluctuations of Bregne ice cap, Scoresby Sund, east Greenland: A proxy for climate along the Greenland Ice Sheet margin. *Quaternary Science Reviews*, 92, 357–368. <https://doi.org/10.1016/j.quascirev.2013.06.024>
- Lowell, T. V., Hall, B. L., Kelly, M. A., Bennike, O., Lusas, A. R., Honsaker, W., Smith, C. A., Levy, L. B., Travis, S., & Denton, G. H. (2013). Late Holocene expansion of Istorvetice Cap, Liverpool Land, East Greenland. *Quaternary Science Reviews*, 63, 128–140. <https://doi.org/10.1016/j.quascirev.2012.11.012>
- Lusas, A. R., Hall, B. L., Lowell, T. V., Kelly, M. A., Bennike, O., Levy, L. B., & Honsaker, W. (2017). Holocene climate and environmental history of East Greenland inferred from lake sediments. *Journal of Paleolimnology*, 57(4), 321–341. <https://doi.org/10.1007/s10933-017-9951-5>
- McKay, N. P., Kaufman, D. S., Routson, C. C., Erb, M. P., & Zander, P. D. (2018). The onset and rate of Holocene neoglacial cooling in the Arctic. *Geophysical Research Letters*, 45, 12,487–12,496. <https://doi.org/10.1029/2018GL079773>
- Medford, A. K., Hall, B. L., Lowell, T. V., Kelly, M. A., Levy, L. B., Wilcox, P. S., & Axford, Y. (2021). Holocene glacial history of Renland Ice Cap, East Greenland, reconstructed from lake sediments. *Quaternary Science Reviews*, 258, 106883. <https://doi.org/10.1016/j.quascirev.2021.106883>
- Oliva, M., Fernandes, M., Palacios, D., Fernández-Fernández, J. M., Schimmelpfennig, I., Antoniades, D., Aumaitre, G., Bourlès, D., & Keddadouche, K. (2021). Rapid deglaciation during the Bølling-Allerød interstadial in the Central Pyrenees and associated glacial and periglacial landforms. *Geomorphology*, 385, 107735. <https://doi.org/10.1016/j.geomorph.2021.107735>
- Palacios, D., Stokes, C. R., Phillips, F. M., Clague, J. J., Alcalá-Reygosa, J., Andrés, N., Angel, I., Blard, P. H., Briner, J. P., Hall, B. L., Dahms, D., Hein, A. S., Jomelli, V., Mark, B. G., Martini, M. A., Moreno, P., Riedel, J., Sagredo, E., Stansell, N. D., ... Ward, D. J. (2020). The deglaciation of the Americas during the last glacial termination. *Earth-Science Reviews*, 203(February), 103113. <https://doi.org/10.1016/j.earscirev.2020.103113>
- Payer, J. (1876). *Die Oesterreichisch-Ungarische Nordpol-Expedition in Den Jahren 1872–1874: Nebst Einer Skizze Der Zweiten Deutschen Nordpol-Expedition 1869–1870, Und Der Polar-Expedition von 1871* (p. 1876). A. Hoelder.
- Pedersen, S. H. (2017). *Scaling-up climate change effects in Greenland*. Aarhus University.
- Porter, C., Morin, P., Howat, I., Noh, M.-J., Bates, B., Peterman, K., Keese, S., Schlenk, M., Gardiner, J., Tomko, K., Willis, M., Kelleher, C., Cloutier, M., Husby, E., Foga, S., Nakamura, H., Platson, M., Michael Wethington, C. W., Jr., Bauer, G., ... Mikkel A4-National Science Foundation A4-National Science Foundation Bojesen. (2018). ArcticDEM.
- Porter, S. C. (2000). Onset of neoglaciation in the Southern Hemisphere. *Journal of Quaternary Science*, 15(4), 395–408. [https://doi.org/10.1002/1099-1417\(200005\)15:4%3C395::AID-JQS535%3E3.0.CO;2-H](https://doi.org/10.1002/1099-1417(200005)15:4%3C395::AID-JQS535%3E3.0.CO;2-H)
- Porter, S. C., & Denton, G. H. (1967). Chronology of neoglaciation in the North American Cordillera. *American Journal of Science*, 265(3), 177–210.
- Prescott, J. R., & Hutton, J. T. (1994). Cosmic ray contributions to dose rates for luminescence and ESR dating: Large depths and long-term time variations. *Radiation Measurements*, 23(2–3), 497–500. ISSN 1350-4487. [https://doi.org/10.1016/13504487\(94\)90086-8](https://doi.org/10.1016/13504487(94)90086-8) <https://www.sciencedirect.com/science/article/pii/S1350448794900868>
- Renssen, H., Seppä, H., Crosta, X., Goosse, H., & Roche, D. (2012). Global characterization of the Holocene thermal maximum. *Quaternary Science Reviews*, 48, 7–19.

- Renssen, H., Seppä, H., Heiri, O., Roche, D. M., Goosse, H., & Fichefet, T. (2009). The spatial and temporal complexity of the Holocene thermal maximum. *Nature Geoscience*, 2(6), 411–414. <https://doi.org/10.1038/ngeo513>
- Reusche, M. M., Marcott, S. A., Ceperley, E. G., Barth, A. M., Brook, E. J., Mix, A. C., & Caffee, M. W. (2018). Early to late Holocene surface exposure ages from two marine-terminating outlet glaciers in north-west Greenland. *Geophysical Research Letters*, 45(14), 7028–7039. <https://doi.org/10.1029/2018GL078266>
- Rule, Home. (2005). British Mountaineering Council, Royal Geographical Society, Domestic Affairs, North-east Green, National Park, Blossville Kyst, Nanu Travel Aps, Kap Tobin, Zackenberg Ecological, Zackenberg Ecological, Nuna Travel Aps, The Sirius, Sledge Patrol, and Sirius Sledge Patrol. 2005. "Exploration History of Northern East Greenland."
- Søndergaard, A. S., Larsen, N. K., Steinemann, O., Olsen, J., Funder, S., Egholm, D. L., & Kjær, K. H. (2020). Glacial history of Ingfield Land, north Greenland from combined in situ 10 Be and 14 C exposure dating. *Climate of the Past*, 16(5), 1999–2015. <https://doi.org/10.5194/cp-16-1999-2020>
- Schweinsberg, A. D., Briner, J. P., Licciardi, J. M., Bennike, O., Lifton, N. A., Graham, B. L., ... Zimmerman, S. H. (2019). Multiple independent records of local glacier variability on Nuussuaq, West Greenland, during the Holocene. *Quaternary Science Reviews*, 215, 253–271. <https://doi.org/10.1016/j.quascirev.2019.05.007>
- Skov, D. S., Andersen, J. L., Olsen, J., Jacobsen, B. H., Knudsen, M. F., Jansen, J. D., Larsen, N. K., & Egholm, D. L. (2020). Constraints from cosmogenic nuclides on the glaciation and erosion history of Dove Bugt, Northeast Greenland. *Bulletin of the Geological Society of America*, 132(11–12), 2282–2294. <https://doi.org/10.1130/B35410.1>
- Stone, J. O. (2000). Air pressure and cosmogenic isotope production. *Journal of Geophysical Research*, 105(1), 753–759. <https://doi.org/10.1029/2000JB900181>
- Vasskog, K., Langebroek, P. M., Andrews, J. T., Nilsen, J. E. Ø., & Nesje, A. (2015). The Greenland ice sheet during the last glacial cycle: Current ice loss and contribution to sea-level rise from a Palaeoclimatic perspective. *Earth-Science Reviews*, 150, 45–67. <https://doi.org/10.1016/j.earscirev.2015.07.006>
- Vinther, B. M., Clausen, H. B., Fisher, D. A., Koerner, R. M., Johnsen, S. J., Andersen, K. K., Dahl-Jensen, D., Rasmussen, S. O., Steffensen, J. P., & Svensson, A. M. (2008). Synchronizing ice cores from the Renland and Agassiz ice caps to the Greenland ice core chronology. *Journal of Geophysical Research Atmospheres*, 113(8), 1–10. <https://doi.org/10.5194/cp-4-47-2008>
- Walker, M., Head, M. J., Berkelhammer, M., Björck, S., Cheng, H., Cwynar, L., Fisher, D., Gkinis, V., Long, A., Lowe, J., Newnham, R., Rasmussen, A. O., & Weiss, H. (2018). Formal ratification of the subdivision of the Holocene Series/Epoch (Quaternary System/Period): Two new Global Boundary Stratotype Sections and Points (GSSPs) and three new stages/subseries. *Episodes*, 41(4), 1–11. <https://doi.org/10.18814/epiugs/2018/018016>
- Young, N. E., Briner, J. P., Miller, G. H., Lesnek, A. J., Crump, S. E., Thomas, E. K., Pendleton, S. L., Cuzzone, J., Lamp, J., Zimmerman, S., Caffee, M., & Schaefer, J. M. (2020). Deglaciation of the Greenland and Laurentide ice sheets interrupted by glacier advance during abrupt Coolings. *Quaternary Science Reviews*, 229, 106091. <https://doi.org/10.1016/j.quascirev.2019.106091>
- Young, N. E., Schaefer, J. M., Briner, J. P., & Goehring, B. M. (2013). A 10Be production-rate calibration for the Arctic. *Journal of Quaternary Science*, 28(5), 515–526. <https://doi.org/10.1002/jqs.2642>

**How to cite this article:** Garcia-Oteyza Ciria, J., Oliva, M., Palacios, D., M. Fernández-Fernández, J., Schimmelpfennig, I., Medialdea, A., Fernandes, M., Giralt, S., Jomelli, V., Antoniadis, D., & ASTER TEAM (2023). Holocene glacial oscillations in the Tyroler Valley (NE Greenland). *Land Degradation & Development*, 34(9), 2589–2606. <https://doi.org/10.1002/ldr.4633>